8260 *Macromolecules* **2009**, *42*, 8260–8270
DOI: 10.1021/ma901584w

Macromolecules
ARTICLE

Multiscale Computer Simulation Studies of Water-Based Montmorillonite/Poly(ethylene oxide) Nanocomposites

Radovan Toth,[†] Dirk-Jan Voorn,[‡] Jan-Willem Handgraaf,[§] Johannes G. E. M. Fraaije,[§,⊥] Maurizio Fermeglia,[†] Sabrina Pricl,[†] and Paola Posocco*,[†]

[†]*Molecular Simulation Engineering (MOSE) Laboratory, Department of Chemical Engineering (DICAMP), University of Trieste, 34127 Trieste, Italy,* [‡]*Fluor Consultants B.V., 3088EA Rotterdam, The Netherlands,* [§]*Culgi B.V., 2300 AN Leiden, The Netherlands, and* [⊥]*Leiden Institute of Chemistry, Soft Matter Chemistry, Gorlaeus Laboratories, Universiteit Leiden, 2333 CC Leiden, The Netherlands*

Received July 20, 2009; Revised Manuscript Received September 8, 2009

ABSTRACT: This work presents a multiscale computational approach to probe the behavior of polymer/clay nanocomposites based on poly(ethylene oxide) (PEO)/montmorillonite (MMT) as obtained from water intercalation. In details, our modeling recipe is based on four sequential steps: (a) atomistic molecular dynamics simulations to derive interaction energy values among all system components; (b) mapping of these values onto mesoscale dissipative particle dynamics parameters; (c) mesoscopic simulations to determine system density distributions and morphologies (i.e., intercalated vs exfoliated); (d) simulations at finite-element levels to calculate the relative macroscopic properties. The entire computational procedure has been applied to four PEO/MMT systems with PEO chains of different molecular weight (750, 1100, 2000, and 5000), and thermal and electrical characteristics were predicted in excellent agreement with the available experimental data. Importantly, our methodology constitutes a truly integrated multiscale modeling approach, in which no "learning against experiment" has been performed in any step of the computational recipe.

1. Introduction

In recent years, polymer nanocomposites based on layered silicates, or polymer−clay nanocomposites (PCNs), have attracted great industrial and academic interest as they often exhibit remarkable improvement in materials properties with respect to virgin polymers or conventional micro/macro composites. These enhanced features include high mechanical moduli, increased strength and heat resistance, decreased gas permeability and flammability, and increased biodegradability in case of biodegradable polymers.[1] Fabricating polymer clay nanocomposites (PCNs) in an efficient and cost-effective manner, however, poses significant synthetic challenges. As the ultimate properties of these hybrid systems commonly depend on their structure, it is of particular interest to establish the morphology of the final composite. To this purpose, the development of theories and the application of computer simulation techniques have opened avenues for the design of these materials, and the *a priori* prediction/optimization of their structures and properties.[2]

The commonly used clay materials for the preparation of PCNs belong to the same general family of 2:1 layered silicates, or phyllosilicates, montmorillonite (MMT) being a prime example of these minerals. Their crystal structure consists of layers made up of two tetrahedrally coordinated silicon atoms fused to an edge-shared octahedral sheet of either aluminum or magnesium hydroxide. The layer thickness is around 1 nm, and the lateral dimension may vary from 30 nm up to several micrometers or larger, depending on the particular mineral. Stacking of the layers leads to a regular van der Waals gap between the layers called the interlayer space or gallery. Isomorphic substitution within the layers (for example, Al^{3+} replaced by Mg^{2+} or Fe^{2+}, or Mg^{2+} replaced by Li^{+}) results in an excess of negative charge, which is counterbalanced by alkali and alkaline earth cations located inside the galleries. This type of layered silicate is characterized by a moderate surface charge known as the cation exchange capacity (CEC), generally expressed as mequiv/100 g.

Generally speaking, mixing a polymer and a clay may not result in a nanocomposite material.[1] Indeed, in their pristine state layered silicates are only directly miscible with hydrophilic polymers, such as poly(ethylene oxide) (PEO)[3] or poly(vinyl alcohol) (PVA).[4] To render layered silicates compatible with other polymer matrices, one must convert the normally hydrophilic silicate surface to an organophilic one, making the intercalation of many engineering polymers possible.

Depending on the strength of interfacial interactions between the polymer matrix and the clay (modified or not), two main types of PCNs can be thermodynamically achieved: (i) intercalated nanocomposites, in which the insertion of a polymer matrix into the clay galleries occurs in a crystallographically regular fashion, regardless of the clay to polymer ratio, and (ii) exfoliated nanocomposites, where the individual clay layers are separated in a continuous polymer matrix by an average distances that depends on clay loading. The two architectures described above can be practically produced by (i) *in situ* polymerization of a given monomer in the presence of the layered silicate, (ii) solution intercalation, where both the polymer matrix and clay are dispersed in a common solvent followed by precipitation, or (iii) melt processing, which involves the mechanical mixing of the polymeric matrix and the inorganic filler.[1b]

MMT/PEO-based PNCs are hybrid structures with improved electrical properties for electronic applications in solid-state electrolyte batteries.[5−7] The intercalation of water-soluble PEO molecules between the clay galleries can be obtained by mixing the clay with an aqueous dispersion of PEO (i), or by direct intercalation from the melt (ii).[8] In the latter case, the organic

*To whom correspondence should be addressed. E-mail: posocco@dicamp.units.it.

 Published on Web 10/06/2009

component is inserted between the clay layers such that the interlayer spacing is expanded to an extent at least sufficient to replace the water of hydration associated with the exchangeable cations in the galleries.[9] An alternative method for the preparation of PEO nanocomposites is the dispersion of completely exfoliated clay particles within the polymer matrix. Under these conditions, the observed behavior is rather different with respect to the one described above: indeed, the addition of an adsorbing polymer to the clay colloidal dispersion can cause flocculation at low surface coverage, and steric stabilization when the particle surface is saturated with the polymer.[10]

As stated above, PCNs offer a wide range of promising applications because of their enhanced properties with respect to the polymeric matrix *per se*. However, further development of such nanomaterials depends on the fundamental understanding of their hierarchical structures and behaviors, a goal which requires multiscale modeling and simulation strategies to provide seamless coupling among various length and time scales. Several computational approaches, spanning different length/time scale domains have been proposed in recent years for the characterization of polymer−clay nanocomposites, including atomistic molecular dynamics (MD) and Monte Carlo (MC), mesoscale, and finite element simulations.[2]

As concerns PEO-based PCNs, it has been more than 20 years since PEO was first suggested as a suitable polymeric matrix for these systems.[11] Accordingly, a plethora of MD-based simulations have been successfully applied to study, for example, the mobility of ions in PEO matrices,[12] segmental motion of polymer backbone in PEO melts,[13] influence of the polarizability in PEO solid electrolytes,[14] and the effect of temperature,[12b,15,16] concentration,[15] solvent,[16] and salt[12b,17] on the dynamics of PEO segments. Further, the effect on polymer dynamics exerted by the addition of methoxy-terminated PEO side-chains with different lengths and separations to an amorphous long-chain PEO backbone has also been studied using MD techniques.[18] As concerns the resulting PCN systems, Aabloo et al. have studied the molecular behavior at the interface between PEO and an inorganic double-layered gel by a molecular mechanics/molecular dynamics (MM/MD) approach.[19] Similarly, PEO inorganic nanocomposites were subject to MM/MD experiments aimed at characterizing the effect of the nanoparticle filler, its concentration, and its temperature on the motion of ions in the polymer host.[15,20] In spite of these efforts devoted to the simulation of PEO-based systems, there is still a lack of studies dealing with computational modeling and simulations of PEO nanocomposites, with special mention to those systems obtained from solution.

In a previous paper from our group,[21] we presented a hierarchical procedure for bridging the gap between atomistic and finite element calculations via mesoscale simulations (MS) in polymer−clay nanocomposite design. According to the proposed computational recipe, the dissipative particle dynamics (DPD)[22] was adopted as the mesoscale simulation technique, and the interaction parameters of the mesoscopic model were estimated by mapping interaction energy values obtained from atomistic MD simulations. Finally, the morphologies and density distributions of the PCN system components were used as input for finite element calculations to estimate the most relevant macroscopical properties.

This work is organized as follows. First, we aimed at studying the interactions which occur at a molecular level near the surface of MMT platelets in PEO aqueous systems. In particular, we focused our attention on the effects of polymer molecular weight, and presence of water molecules on the interactions between individual PCN components. Second, we expanded the information obtained from the atomistic simulations by employing mesoscale models for density profiles and morphology predictions. To this purpose, the resulting MD data were mapped onto the corresponding mesoscale models, and the results generated at both length scales were compared for consistency. Lastly, the density profiles and the morphologies resulting from the MS simulations were imported into a finite element code, and some characteristic macroscopic properties of these systems—e.g. thermal expansion coefficients and electrical conductivity as functions of PEO molecular weight and clay loading—were predicted and compared with the corresponding experimental values available in the current literature.

To the best of our knowledge, this is the first attempt to study the behavior of water molecules in nanocomposites at the mesoscale level and to estimate macroscopic properties for water-based PEO PCNs via multiscale molecular modeling procedures.

2. Computational Methodology

Atomistic Models and Simulations. All atomistic simulations were performed using *Materials Studio* (v.4.3, Accelrys, San Diego, CA). The starting structure of sodium montmorillonite (MMT) was taken from our previous work.[23] As mentioned above, one of the major goals of this work was to estimate the interaction energies between all system elements accurately. Since these quantities are highly sensitive to the nonbonded components of the force field (FF) employed (e.g., atomic charges and van der Waals parameters), here we adopted the *ad hoc* force field developed by Heinz and co-workers.[24] As demonstrated by the authors[24] for sodium MMT and other phyllosilicates, this accurately derived FF is able to describe, among many other properties, the thermodynamics of surface processes more reliably by reducing deviations of 50−500% in surface and interface energies to less that 10%, which constitutes a fundamental step toward quantitative modeling of interface processes involving layered silicates. Accordingly, the resulting lattice of our MMT model is monoclinic, with space group $C2/m$, and characterized by the following lattice parameters: $a = 5.20$ Å, $b = 9.20$ Å, $c = 10.13$ Å, and $\alpha = 90°, \beta = 99°, \gamma = 90°$, in excellent agreement with the available literature.[24b,25]

The generation of PEO chains was conducted following a well-validated procedure,[23] according to which the constitutive repeating unit (CRU) of the polymer was first built and its geometry optimized by energy minimization again using PCFF. Hence, the CRU was polymerized to a given degree of polymerization (DP). Four different values of DP were considered in order to study the influence of PEO molecular weight (M_W) on the interaction energies of the corresponding PCN systems: DP = 19, 28, 56, and 113, approximately corresponding to a M_w of 750, 1100, 2000, and 5000, respectively. The rotational isomeric state (RIS) algorithm,[26] as modified by Theodorou and Suter,[27] was used to create the initial polymer conformations at $T = 300$ K. Explicit hydrogens were used in all model systems. In order to obtain a reasonable sampling of the polymer conformational space, we built and energy minimized 10 different PEO configurations for each DP considered. A conformational search was then carried out using our well-validated combined molecular mechanics/molecular dynamics simulated annealing (MDSA) protocol,[23,28] in which the relaxed molecular structure is subjected to five repeated temperature cycles using constant volume/constant temperature (*NVT*) MD conditions. At the end of each annealing cycle, the structure is again energy minimized, and only the structure corresponding to the minimum energy is used for further modeling.

Resorting to atomistic MD simulations in the canonical ensemble allows retrieving important information on the interaction and binding energy values between the different components of a PCN system.[20,23,28f,30−32] The technique basically consists in simulating the interface between the exfoliated clay, polymer and water by building a cell that is "stretched" along the *c*-direction. Accordingly, a MMT supercell of 10 × 5 × 2

(~5.2 nm × 4.6 nm × 2.3 nm) was first constructed. For each of the 10 different PEO conformations obtained in correspondence of a given DP, we copied six PEO chains with DP = 19, four chains with DP = 28, two chains with DP = 56, and 1 chain with DP 113 in 10 identical MMT supercells, thus obtaining 40 different binary model systems (10 for each DP) overall. This choice allowed for an approximately constant number of polymer atoms in each simulation cell, a condition necessary for energy comparison (see below). Each resulting (MMT/PEO) binary system was shortly energy minimized to relieve close contacts. To avoid crystal structure deformation during minimization, both montmorillonite layers were treated as rigid bodies by fixing all cell dimensions, and all atoms in the interlayer space including the cations were allow to move without any constraint.

For the construction of the water-based systems, the SPC/E model was chosen to represent water molecules.[33] Each ternary simulation model consists of a MMT unit cell, the PEO chain(s) with a given DP, and a suitable number of water molecules. Water molecules were added according to the following procedure:[34] first, a MMT cell with a interlayer spacing of 17.6 Å with the PEO chain(s) inserted in the interlayer space was created, and a short (50 ps) MD simulation was performed to equilibrate the polymer configuration within the MMT gallery. Then water was adsorbed through a grand canonical Monte Carlo (GCMC) simulation, in which chemical equilibrium was established by imposing vapor pressure of 100 kPa (1 atm). The corresponding hydrated system was equilibrated with another, short NVT MD run. The water molecules were subsequently deleted and readsorbed through a second GCMC run that ensured the accurate amount of adsorbed water.[35]

To generate a mineral surface apt for the simulation, the top silicate sheet, along with the appropriate number of alkali ions, was moved along the *c* cell axis up to 150 Å.[23,28f,29] This extension in the *c*-direction, being quite larger than the maximum system length, results in an effective 2D (*x,y*) periodic system,[36] which allows the use of the *NVT* ensemble for successive molecular dynamics (MD) simulations instead of the alternative constant-pressure constant-temperature (*NPT*) ensemble. As pointed out by previous studies,[37] the small difference in the pressure component along the *z* axis (P_{zz}), relative to the *NPT* ensemble, is negligible; furthermore, the uncertainties in selecting the correct barostat are eliminated, and the required computational time is reduced. The new equilibrium position of the remaining Na^+ counterions on the remaining MMT sheet were determined following the procedure suggested by Heinz et al.[24b] Accordingly, half of them were placed 1 nm away on one side, and the remaining half 1 nm away on the other side of the MMT layer in 10 different arrangements; molecular mechanics energy minimizations were then performed to convergence, keeping all other MMT atoms fixed, and the structure with the lowest energy was finally selected for further simulations. In this configuration, the Na^+ ions are found at about 1.8 Å from the center of the surface oxygen atoms, or about 4.8 Å from the central plane of the metal atoms, in excellent agreement with previous simulations,[34] and experimental NMR data.[38] In fact, surface lattice cavities are characteristic of the oxygen network in all 2:1 layer silicates, and in cations primarily reside partially inserted within these cavities.

Subsequently, 500 ps of NVT MD experiments were run at 300 K for each system, using the Verlet algorithm and an integration step of 1 fs. The Ewald summation method[39] was applied for treating both van der Waals and electrostatic interactions. Temperature was controlled using the Nosé thermostat.[40] (*Q* ratio = 1). In order to reduce computational time, during each MD both montmorillonite layers were treated as rigid bodies by fixing all cell dimensions, and all atoms in the interlayer space including the cations were allow to move without any constraint. The total number of ternary systems generated was 40, 10 for each PEO DP value considered.

The procedure used to calculate the interaction energies and, hence, the binding energy values E_{bind} between all system components, is described in details in our previous papers.[21,23a−d,28f] By definition, the binding energy E_{bind} is the negative of the interaction energy. As an example, to calculate the binary binding energy term $E_{bind}(PEO/H_2O)$, we can first created a PEO−H_2O system deleting the MMT platelet and the Na^+ ions from one of the equilibrated MD trajectory frames, and then calculated the potential energy of the system E_{PEO/H_2O}. Next, we deleted the water molecules, leaving the PEO chain alone, and thus calculated the energy of the PEO molecule, E_{PEO}. Similarly, we deleted the PEO molecules from the PEO−H_2O system, and calculated E_{H_2O}. Then, the binding energy $E_{bind}(PEO/H_2O)$ is simply obtained from the following equation:

$$E_{bind}(\mathrm{PEO/H_2O}) = E_{PEO} + E_{H_2O} - E_{PEO/H_2O} \quad (1)$$

The remaining binding energy terms, E_{bind}(PEO/MMT) and E_{bind}(MMT/H_2O), can be calculated in an utterly analogous fashion from the corresponding energy components.

As the MD frames choice is concerned, we decided to calculate the system energies at 300, 350, 400, 450, and 500 ps. We considered these as representative energy values,[21] since every energy component was well equilibrated after approximately 100 ps of simulation. All data collected have then been averaged over the 10 different model systems for each PEO DP.

Importantly, the binding energies between the individual components of each nanocomposite system estimated using the procedure outlined above will also constitute the input parameters for the higher level, mesoscale simulations, as described in the next section.

In order to investigate the arrangement of PEO and water molecules in the silicate galleries along a plane normal to the mineral surfaces, and to compare these with the corresponding morphology resulting from mesoscale simulations (see below), we applied an original procedure to simulate PEO chains intercalation into the clay galleries. For the simulations, we used the same molecular models employed in the *NVT* binding energies calculations described above. Starting from the 10 × 5 × 2 MMT supercell, we performed a geometry optimization of the system, keeping all cell parameters fixed except for the *c* distance, and using a convergence criterion of 10^{-4} kcal/(mol Å). The resulting configuration was then subjected to the MDSA procedure, in order to sample as many system configurations as possible. The total simulation lasted 25 ps, with a time step of 1 fs, and consisted of five annealing cycles with a starting temperature of 300 K, a midcycle temperature of 1500 K, and five heating ramps per cycle. The Ewald method[39] was again employed for treating the nonbonded energy components, and the Nosé thermostat[40] was chosen for temperature control. After each cycle, a molecular geometry optimization was run with the same criteria described before. Finally, the lowest potential energy conformation from the five different frames obtained as output from the described procedure was selected for further modeling. This frame was used as an initial configuration for the polymer chain/water molecules insertion. To this purpose, we used the different PEO chains built as reported in the previous section, and the same water adsorption recipe. After each polymer chain/s and water insertion, we performed the optimization procedure described above. The final systems were subjected to the last *NVT* annealing run, from which we selected the lowest potential energy frames from the trajectory files and used them as starting configurations to perform productive 300 ps *NVT* runs. Once the simulations were completed, 30 frames were extracted from the corresponding trajectory files, and on each one we performed the density profile calculations within the interlayer spaces.

Mesoscale Models and Simulations. In order to obtain the morphology of polymer and water molecules between the

montmorillonite layers, and to evaluate and compare the influence of the polymer molecular weight at a mesoscopic level, dissipative particle dynamics (DPD)[22] simulations were carried out using the *DPD module* of the Culgi modeling suite (Culgi B.V., Leiden, The Netherlands).

In the dissipative particle dynamics simulation method, a set of particles moves according to Newton's equation of motion and interacts dissipatively through simplified force laws. Also, in the DPD model individual atoms or molecules are not represented directly but are coarse-grained into beads. These beads, or particles, constitute local "fluid packages" able to move independently.

The force acting on the beads, which is pairwise additive, can be decomposed into three elements: a conservative ($\mathbf{F}_{ij}^C$), a dissipative ($\mathbf{F}_{ij}^D$), and a random ($\mathbf{F}_{ij}^R$) force.[41] Accordingly, the effective force $\mathbf{f}_i$ acting on a particle i is given by

$$\mathbf{f}_i = \sum_{i \neq j} (\mathbf{F}_{ij}^C + \mathbf{F}_{ij}^D + \mathbf{F}_{ij}^R) \tag{2}$$

where the sum extends over all particles within a given distance r_c from the ith particle. This distance practically constitutes the only length scale in the entire system. Therefore, it is convenient to set the cutoff radius r_c as a unit of length (i.e., $r_c = 1$), so that all lengths are measured relative to the particles radius.[41]

In the framework of a multiscale approach to PCN simulation, the conservative interaction parameters a needed as input for the mesoscale level DPD calculations can be obtained by a mapping procedure of the binding energy values between different species obtained from simulations at a lower (atomistic) scale.[21,23c] The first step necessary for determination of the DPD input parameters generally consists of defining the DPD bead dimensions, thus implicitly defining characteristic length of the system (r_c). The interaction range r_c sets the basic length scale of the system; in other terms, r_c can be defined as the side of the cube containing an average number ρ of beads. Therefore

$$r_c = (\rho V_b)^{1/3} \tag{3}$$

where V_b is the volume of a DPD bead. It is important to recall here that, even in a heterogeneous system consisting of several different species such as a PCN, a basic DPD assumption is that all bead types (each representing a single species) must be of a comparable volume, V_b.

Starting mesoscale model generation with the polymer chain, the basic strategy to calculate the volume of a DPD bead V_b consists in mapping the real polymer chain onto a chain consisting of Kuhn segments. Consequently, each DPD bead represents a statistically correlated unit or Kuhn segment of the polymer. A DPD chain should, therefore, be made up of N_{DPD} beads, where

$$N_{DPD} = \frac{N_{mon}}{C_\infty} \tag{4}$$

where N_{mon} is equal to the degree of polymerization of the molecular chain DP and C_∞ is its characteristic ratio. If so, the mesoscale simulations should capture in a reliable way two essential features of a given polymer chain, namely its dimension (given by N_{mon}) and flexibility (given by C_∞). When a flexible macromolecules is modeled as a Gaussian chain, however, C_∞ represents also the number of monomers making up a Kuhn segment (i.e., contained in a single DPD bead). Therefore, the bead volume V_b can be simply obtained multiplying the characteristic ratio C_∞ by the monomer volume V_{mon}, here estimated to be equal to 52.68 Å^3 by the Connolly algorithm.[42]

For a polymeric chain, the characteristic ratio is defined as

$$C_\infty = \frac{\langle R_0^2 \rangle}{N l^2} \tag{5}$$

Table 1. Characteristics of the DPD Beads and Chains Used in This Work

		N_{DPD}[c]			
V_b[a] (Å^3)	r_c[b] (Å)	PEO19	PEO28	PEO56	PEO113
262	9.23	4	6	11	23

[a] DPD bead volume. [b] Cutoff radius. [c] Total number of DPD beads in each PEO chain.

where R_0 is the unperturbed mean-square end-to end distance, N is the total number of skeletal bonds, and l^2 is the mean-square bond length. In the case of PEO, N is three times the degree of polymerization, and l^2 is calculated to be equal to 2.14 Å by simply applying:

$$l^2 = \frac{l^2(\mathrm{C-C}) + 2l^2(\mathrm{C-O})}{3} \tag{6}$$

where C−C = 1.53 Å and C−O = 1.43 Å.[43,44] A conformation-related property such as C_∞ can be experimentally estimated, for example, in dilute polymer solution under unperturbed or θ-conditions or calculated, as done in this work, using a molecular dynamics procedure based on the rotational isomeric state (RIS) method.[45,46] Generally speaking, for a given polymer at low degree of polymerization the characteristic ratio varies with N. According to our simulations (data not shown), we found that, for PEO, C_∞ is only weakly varying with molecular weight, and the average value resulting from the application of the RIS procedure is equal to 4.9. This finding is in good agreement with the corresponding values available in the literature both from experiments and simulation.[43,44,47,48]

The resulting values of the calculated bead volume V_b, the corresponding number of beads for each PEO chain N_{DPD}, and the cutoff radius r_c used in the DPD simulations are listed in Table 1.

Having determined the bead size, and fixed the system density to $\rho = 3$, the characteristic dimension of the mesoscopic system could be calculated from eq 3 as $r_c = 9.23$ Å^3. As said, this value represents the soft potential cutoff distance, but also sets the length of the DPD simulation box. Our overall DPD system was chosen to be constituted by $20 \times 20 \times 3$ unit cells, and hence was characterized by effective dimensions of 18.5 nm × 18.5 nm × 2.8 nm.

At this point, the number of DPD beads of each individual system component (i.e., MMT, PEO, and H_2O) must be estimated. To this purpose, the PEO-based PCN can be devised as composed of three different species of beads: one for the polymer chains (P), one for the water molecules (W), and one for the MMT surface (M). The modeling of the MMT layers in the context of DPD has been addressed by freezing locally the particles representing the silicate solid boundaries. These particles behave as fluid particles but maintain a fixed position and possess zero velocity. Therefore, these MMT walls interacts with each bead in the system with a potential of the same form as the bead−bead conservative force. This force is short-ranged, so the system beads are not strictly forbidden from passing through the barrier. To prevent particles from entering the wall region, several methods have been proposed. In his work, we decided to apply the bounce-forward reflection approach[49] in all calculations. Lastly, the number of individual polymer (Table 1) and water beads can be easily obtained from the atomistic polymer/water molecular volume ratio.

The next, important issue of a DPD simulation is the determination of the bead interaction parameters. The detailed procedure for obtaining these mesoscale interaction parameters from atomistic molecular dynamics binding energies is reported in details elsewhere.[21,23c] Adapting this recipe to the present system, the bead−bead interaction parameter for water−water interaction was set equal to $a_{WW} = 25$, in agreement with the correct value for a density value of $\rho = 3$.[41] The clay-water

Table 2. Bead−Bead Interaction Parameters obtained for Water-Based PEO−MMT Nanocomposites

	P					
a_{ij}	PEO19	PEO28	PEO56	PEO113	*W*	*M*
P	29.7	30.4	30.8	31.2		
W	24.1	26.0	28.1	30.0	25	
M	17.4	16.0	14.6	12.8	15	0

interaction parameter was set to a lower value (i.e., $a_{MW} = 15$), in order to mimic the good affinity between the silicate and water. Once these two parameters were set, and their values associated with the corresponding values of the self-and mixed rescaled DPD energies, all the remaining bead−bead interaction parameters for the DPD simulation could be easily obtained, starting from the atomistic binding energy values, as described previously.[21,23c] The entire set of DPD interaction parameters employed in this work are summarized in Table 2.

In the framework of a multiscale modeling approach, one of the most important outputs of the mesoscale level calculations is the obtainment of the three-dimensional density profiles for each type of bead or, in other words, the system morphology. In fact, these density profiles constitute the input information for the last recipe step: the finite element calculations to estimate macroscopical properties.

Finite Elements Calculations of Macroscopic Properties. Prediction of macroscopic properties of the PEO/MMT PCNs considered in this work, as a function of polymer molecular weight and clays loading, constitutes the final step of our multiscale modeling recipe. To this purpose, finite element (FE) simulations at ordinary temperature were performed using the software Palmyra (v. 2.5, MatSim, Zürich, CH). This software has been validated on different composite material morphologies by several authors, including us,[23c,e50,51] yielding reliable results. FE calculations were applied in order to analyze both platelet stacks and overall nanocomposite properties, using fixed and variable grid, respectively. In particular, thermal expansion coefficients and electrical conductivity were the macroscopic properties of election, since it is in these performances that lies most of the industrial interest toward these new materials. The properties of the pure system components (i.e., silicate, polymer, and water) were taken from the available literature.[52]

One of the major concerns in creating a suitable model for FE calculations is the definition of an appropriate reactive volume element (RVE), which could be representative of the different morphologies characterizing such complex materials as PCNs. Since most of the effects exerted by layered silicate addition is generally observed at low clay contents, we decided to adopt the following values for clay loading: 1%, 2%, 3%, 4%, and 5% w/w. Given the PEO and MMT experimental density values (1.14 and 2.71 g/cm^3, respectively),[52,53] these amounts correspond to clay volume fraction V_f ranging from 2.2% to 0.42%. Relying on previous studies,[23c,e] and on extensive trials (data not shown), we selected to simulate an RVE made up of 48 MMT particles, grouped in stacks of different size, representing both the exfoliated and intercalated states (*vide infra*).

MMT particles (both single particles and stacks) were modeled as disks with a toroidal rim. Each platelet thickness was defined by the height of the corresponding symmetry axis *h* and diameter *d*, thus being characterized by an aspect ratio of $a = d/h$. By setting $d = 120$ nm and $h = 1$ nm for each single particle, the aspect ratio *a* was equal to 120, a value in agreement with common literature data for layer silicates.[1] According to these settings, the volume of a single MMT platelet is $V_p = 11.3 \times 10^3$ nm^3; this information, coupled with the MMT V_f values for each loading and the number of MMT sheets in each model box, was used to retrieve the dimensions of the FE cubic calculation cells.

The mixed nature of intercalation and exfoliation of PEO/MMT PCNs was accounted for by grouping some MMT platelets in stacks; in other words, the models contained two different elements: single MMT sheets, representing exfoliated nanoparticles, and polymer intercalated MMT sheets (or stacks). Stacks were modeled using the same particle representation employed for MMT isolate sheets, but varying the platelet thickness according to the number of sheets characterizing each stack element. As PEO/MMT systems are known to be highly intercalated,[52,54] based on our previous studies,[23c,e] and on the *d*-spacing of stacks resulting from our lower-scale simulations, we convene to represent a PCN characterized by a low exfoliation/high intercalation morphology according to the conditions reported in Table 4. Single particles and stacks were then oriented in the FE simulation box according to a method reported previously.[23c]

Table 3. Binding Energies in Water Systems with PEO Chains of Different Molecular Weight, Where All Energy Values Are Expressed in kcal/mol

	system MMT/PEO/H_2O			
polymer	E_{bind}(MMT/PEO)	E_{bind}(MMT/H_2O)	E_{bind}(PEO/H_2O)	N_A[a]
PEO19	−695	−5300	−891	810
PEO28	−761	−5276	−861	792
PEO56	−898	−5205	−784	788
PEO113	−1015	−5104	−641	798

[a] Total number of polymer atoms in each simulation cell.

Once all model systems were prepared, appropriate surface and volume meshes had to be generated in order to run Palmyra solver and retrieve the macroscopic properties of interest. Mesh generation and refinement methods in Palmyra are quite complex, and their thorough description is beyond the scope of the present work. By applying a displacement-based finite element method to the total mesh, the responses to external deformations were calculated. In order to calculate thermal expansion coefficients, a thermo-elastic solver was used, and a seventh "deformation" (an increase of temperature by 1 K) was applied in order to obtain the linear thermal expansion coefficients. For other physical properties such as electrical conductivity, a Laplace solver was employed, that applies a field in the three main directions to the finite element mesh, and minimizes the energy of the composite.[55]

3. Results and Discussion

Atomistic MD Simulations. In order to study the effect of PEO molecular weight and of the presence of water molecules on the interactions between polymer and clay platelets, we performed atomistic MD simulations of PEO-based PCNs in a solvated environment using polymers of different chain length but with an approximately constant total number of atoms. Accordingly, we modeled 6 PEO chains with a degree of polymerization DP equal to 19, four chains with DP = 28, two chains with DP = 56, and one chain with DP = 113, respectively, approximately corresponding to a molecular weight of 750, 1100, 2000, and 5000. parts a and b of Figure 1 show two MD snapshots of the hydrated MMT/PEO systems with the lowest and highest polymer M_w considered, respectively. The resultant binding energy values between the individual system components are listed in Table 3, from which it can be readily seen that the favorable interactions between clay and polymer, as quantified by the term E_{bind}(MMT/PEO), increase with increasing polymer molecular weight. Thermodynamic arguments can be invoked to account for this trend. Indeed, it can be argued that the PEO macromolecules would generally adopt a conformation that allows for maximum segment-surface interactions.[56] For a given amount of polymer, the number of polymer segments can be assumed to be approximately the same. A higher molecular mass PEO possesses the potential

Table 4. Platelet Stacking Parameters *a* and Relative Aspect Ratio for a Low Exfoliation/High Intercalation Morphology of PEO/MMT PCN Systems[a]

particle type	no. of particles	*a*
single	4	120
2-stack	8	15
4-stack	4	7.5
6-stack	2	5

[a] The term particle designates both single, exfoliated clay sheets and intercalated stacks.

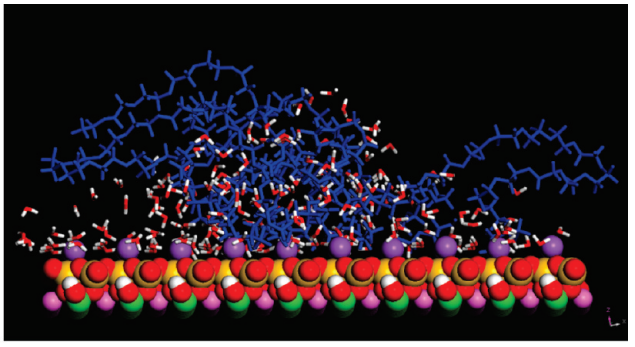

(a)

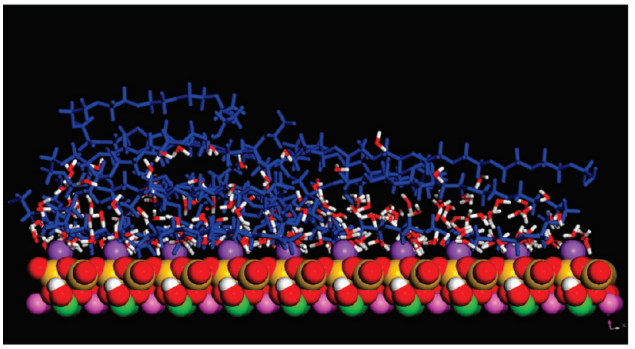

(b)

Figure 1. Equilibrated MD trajectory frames for pseudo 2D solvated MMT systems with (a) 6 PEO chains of DP = 19 and (b) 1 PEO chain of DP = 113, respectively. MMT is represented in CKP style, the polymer is depicted in blue stick rendering, and water molecules are shown as atom-colored sticks. Color legend: gold, silicon; red, oxygen; white, hydrogen; purple, Na; pink, Al; light green, Mg.

to realize larger segment/MMT surface contacts, which favor surface adsorption and, ultimately, result in the highest level on polymer intercalation into the silicate galleries.

Also, montmorillonite as a inorganic mineral is generally considered as being hydrophilic.[57] Nonetheless, the basal Si−O groups in the spaces between hydrated cations in the clay interlayers are relatively hydrophobic, and, as results from the inspection of the corresponding density distribution profiles (*vide infra*), and in line with some other simulation and convincing experimental evidence,[35,58] PEO tends to adsorb preferentially on these sites. A low molecular mass PEO chain features a higher number of hydrophilic −OH end groups with respect to a high molecular mass one; this, in principle, should facilitate the preferential intercalation and adsorption of the longer PEO chains with respect to the smaller ones, for which, conversely, the contact with the MMT are fewer and the chains tend to cluster, with water, in the middle of the interlayer space.

In harmony with the foregoing discussion, both interaction energy terms between clay and water (E_{bind}(MMT/H_2O) and polymer and water (E_{bind}(PEO/H_2O)) decrease with increasing polymer chain length. Generally speaking, water molecules preferably reside on the surface of the clay, by virtue of strong Coulombic interactions between the water dipoles and the charged MMT surface. Further, a number of water molecules are engaged in hydrogen bonds with the surface −OH groups of the MMT platelet as well as with the −OH moieties of the PEO chains. As the chain molecular

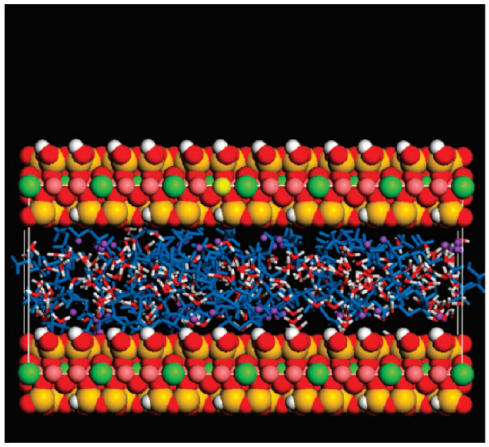

(a)

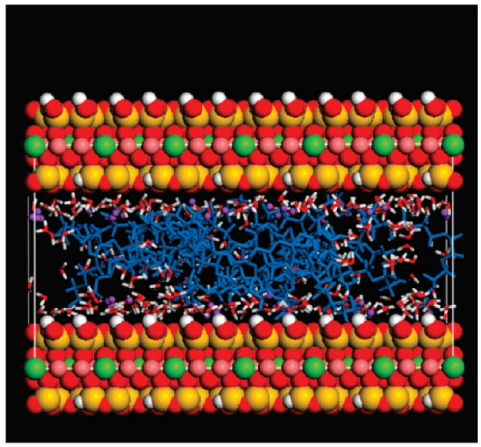

(b)

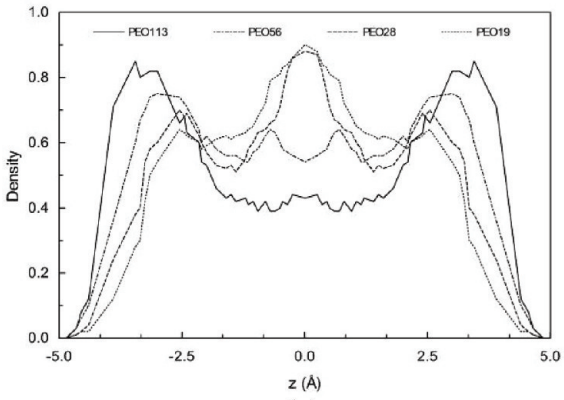

(c)

Figure 2. Starting frame (a) and equilibrated MD trajectory frame for a solvated MMT systems with 6 PEO chains of DP = 19. Molecule representation and color scheme as in Figure 1. (c) Number density profiles of PEO with different DP in solvated MMT nanocomposites: continuous line, PEO DP = 113; dotted-broken line, PEO DP = 56; broken line, PEO DP = 28; dotted line, PEO DP = 19.

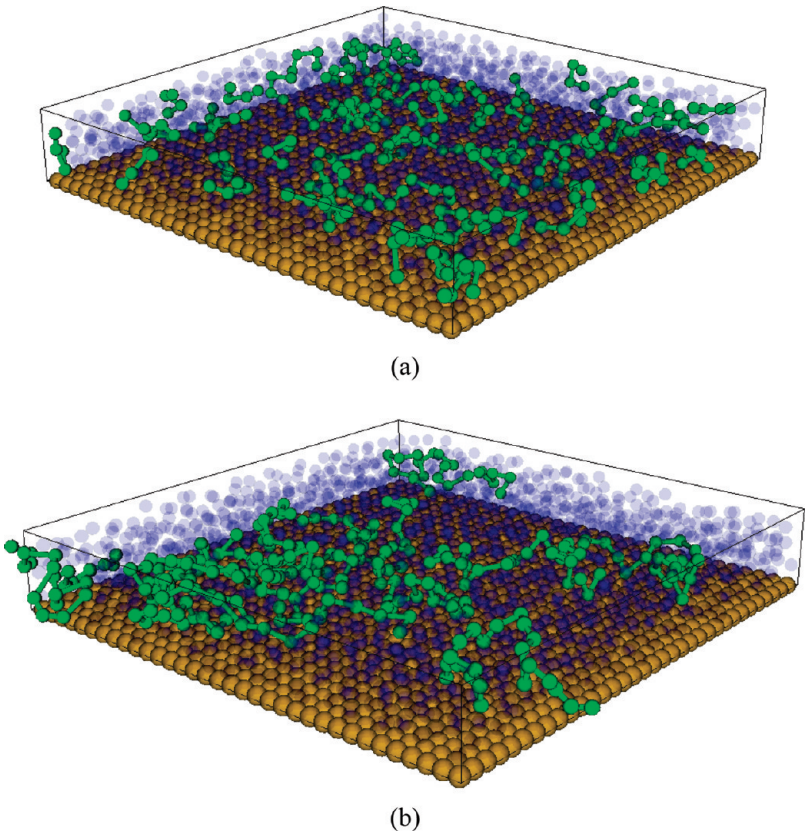

Figure 3. Equilibrated mesoscale morphologies for (a) a solvated MMT systems PEO chains of DP = 19 and (b) a solvated MMT systems with PEO chains of DP = 113. PEO molecules are shows as green sticks-and-balls, MMT walls are portrayed as gold balls, and water molecules are depicted as transparent blue spheres. The top MMT sheet is not shown for clarity.

mass increases, however, less MMT surface is available for water contacts due to a more extensive coverage from the long PEO chains; accordingly, E_{bind}(MMT/H_2O) becomes lower. Also, the decreased hydrophilic character of longer PEO macromolecules with respect to shorter ones reflects in the lower interaction energy values (see Table 3).

Further molecular dynamics simulations were conducted to derive number density profiles, showing the arrangement polymer molecules in the clay galleries, through a plane normal to the silicate galleries, again as a function of the PEO M_w. Parts a and b of Figure 2 show, as an example, the starting configuration and an equilibrated MD frame of the solvated MMT/PEO nanocomposite with PEO chains of molecular mass equal to 750, respectively. Interestingly, the equilibrium interlayer spacing, or *d*-spacing, is relatively insensitive to the degree of polymerization, being equal to 18.2, 18.0, 17.9, and 17.7, for M_w 750, 1100, 2000, and 5000, respectively. These values are in excellent agreements with both experimental and other simulation studies.[34,54,59] A slightly higher *d*-spacing is obtained for the lowest M_w PEO PCN system, an evidence which could be rationalized by the decreasing concentration of available −OH end groups as M_w increases. Also, the preferential location for smaller chains in the middle region of the interlayer space can account for this (albeit small) larger value of *d* (see Figure 2a). Interestingly, Na^+ cations in all cases were found located close to the surface of the mineral platelet, although a number of them were also observed at some distance from the MMT sheets (see Figure 2b), again in agreement with previous studies.[59]

Figure 2c illustrates the density profiles within the silicate galleries as obtained from all PEO samples considered. As can be inferred from this Figure, the density profiles of the polymer carbon atoms change from those typical of a bilayer structure, featuring maxima near the clay platelets and a flat region in the middle in the intergallery space (highest M_w PEO sample), to those pertaining to a trilayer structure, in which some chains still remain in the vicinity of the mineral surface but a substantial part of the material tends to concentrate in the middle of the MMT interlayer (lowest M_w PEO sample). As discussed above, high mass PEO chains feature the highest binding energy with the MMT surface (see Table 3). In line with this evidence, these longer macromolecules tend to align themselves parallel to the clay wall, so that the highest number of chain segments can line up in a single layer and, thus, maximize the number of favorable contacts with the mineral. Quite an opposite situation is encountered at the other extreme of PEO molecular mass values considered in our study. Indeed, the high number of hydrophilic −OH chain ends tend to limit contacts with the basal Si−O groups, and improve the number of the more favorable water-polymer contacts (see Table 3), a situation which can be aptly realized by confining a consistent amount of PEO in the central part of the clay intergallery space. Finally, a smooth, continuum transition between these two extremes is seen for the remaining two intermediate M_w PEO PCN, again in line with the progressively decreasing valued of the corresponding E_{bind}(MMT/PEO) values listed in Table 3.

Mesoscopic Simulations. By using the dissipative particle dynamics approach along with the interaction parameters obtained from lower scale (i.e., atomistic MD) simulations as described in the Materials and Methods section, we modeled and simulated all solvated MMT/PEO PCNs at a mesoscopic level. In harmony with the MD approach, to mimic polymers of different M_w we simulated four types of

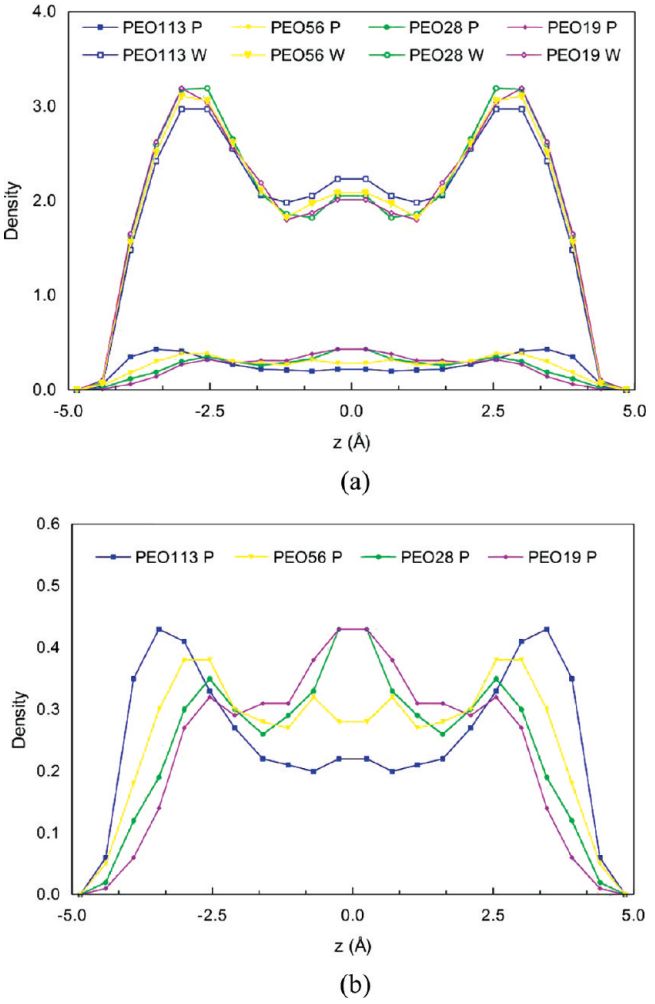

Figure 4. (a) DPD mesoscale density profiles of the interlayer polymer/water phase in the direction normal to the clay layers for water and polymer at different molecular weight. (b) Same data but without water curves for a better appreciation of the polymer density distribution. Legend: full symbols, polymer; empty symbols, water; blue squares, PEO with DP = 113; yellow triangles, PEO with DP = 56; green circles, PEO with DP = 28; purple diamonds, PEO with DP = 19.

PEO chains with different number of beads; the total number of PEO beads, however, was kept constant in all systems. Parts a and b of Figure 3 illustrate the system morphologies obtained from these simulations for the lowest and highest M_w PEO solvated PCN system, as an example. A cursory comparison of Figure 3b with Figure 2b reveals a very good agreement between atomistic and mesoscale predictions. In fact, the highest tendency to flatten onto the MMT surface for the longer PEO with respect to preferred water contacts for chains of lower mass is well preserved at the scale level.

A quantitative analysis of these systems can be carried out by considering the density profiles along the direction normal to the silicate surface, which are reported in Figure 4, parts a and b. The shape of all density curves reveal the high but different affinity of polymer and water molecules for the inorganic surface: indeed, the density of water beads near the MMT surface is higher than that of the polymer chains (see Figure 4a), in agreement with the results gathered from MD simulations, again indicating that water molecules preferably reside on the surface of the clay. Also, the density profiles of polymer beads in the DPD simulation box (see Figure 4b) clearly confirm the predictions obtained

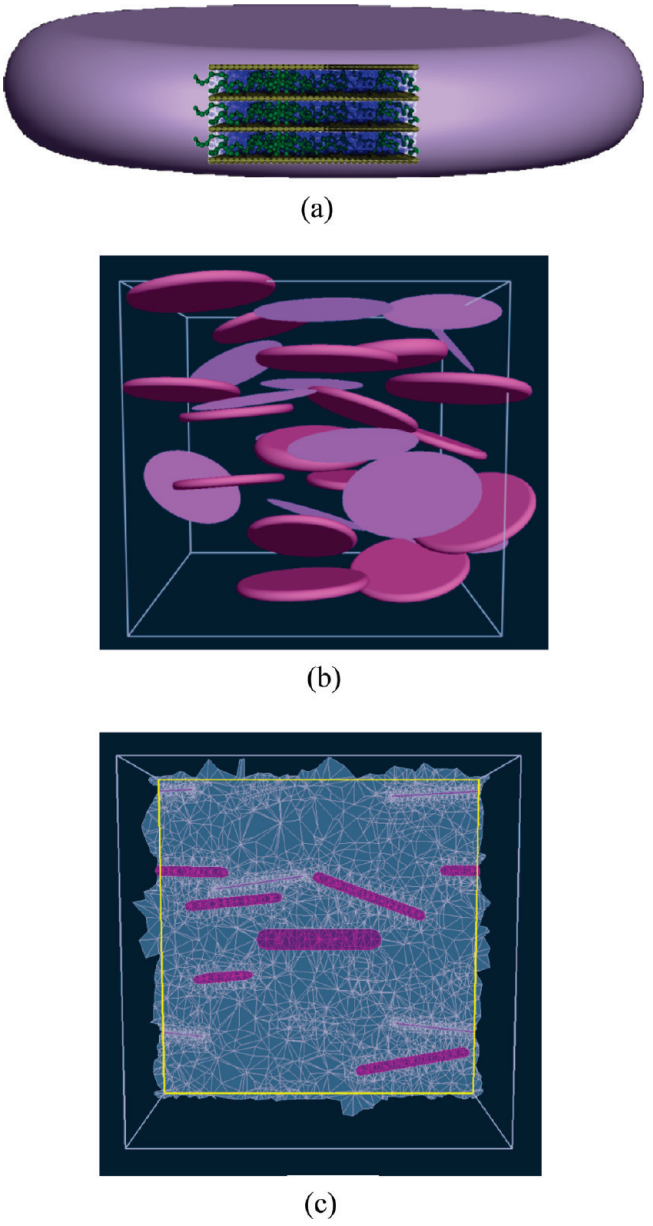

Figure 5. Intercalated stack in the FE RVE model of the PEO/MMT PCN (a), global model configuration (b), and relative meshed volume (c) used in the FE calculations for the PEO/MMT system with PEO of M_w = 5000 and 5% clay loading.

from the lower scale simulation that higher molecular weight polymers possess a higher affinity for the MMT surface. In fact, the density of polymer chains near the clay surface increases with increasing polymer chain length. This effect progressively levels out as the polymer chain decreases in length, and a further maximum in the density profile correspondingly appears, located in the clay gallery middle space, in harmony with the corresponding MD quantitative results.

Finite Element Estimation of Macroscopic Properties. Polymer−clay nanocomposites in which an hydrophilic polymer, such as PEO, is highly intercalated within the sheets of layered silicates such as sodium/lithium MMT show interesting electromechanical responses, rendering them potential candidates for applications as electrolytes in, for instance, solid batteries.[5−7] Accordingly, for FE calculations we decided to focus on the predictions of those macroscopic properties of PEO/MMT systems most relevant to these

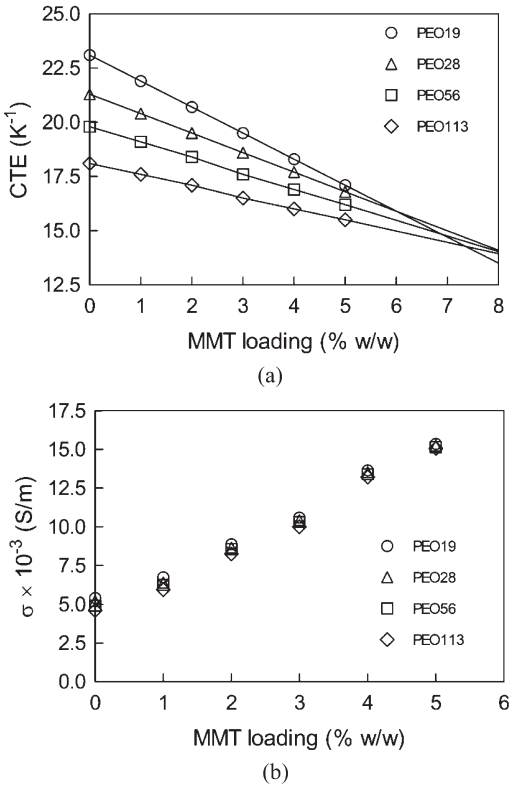

Figure 6. Coefficient of thermal expansion (CTE) (a) and electrical conductivity σ (b) for all PEO/MMT PCNs as a function of clay loading, as predicted from finite element calculations based upon the multiscale modeling procedure developed in this work.

practical purposes, i.e., thermal expansion coefficients and electrical conductivity. To this end, we took into consideration the dependence of these properties on the PEO M_w (in the range 750−5000) and on the MMT loading (between 1% and 5% w/w). Parts a−c of Figure 5 illustrate an intercalated stack in the FE RVE model of the PCN, a global model configuration, and the relative meshed volume used in the FE calculations for the PEO/MMT system with PEO of M_w = 5000 and 5% clay loading, as an example.

The results of the FE calculations for the coefficient of thermal expansion (CTE) for the different PEO/MMT as a function of clay loading are shown in Figure 6a. As can be seen from this image, the values of CTE linearly decrease as MMT loading increases, for all molecular weight PEOs, in agreement with available experimental evidence on closely related systems.[60] The linear thermal expansion of a nanocomposite will greatly depend on the average orientation of the platelets. The effect of inorganic filler orientation on the reduction of linear thermal expansion is similar to the effect on modulus enhancement or reinforcement which has been studied more extensively. Filler geometry can also greatly affect physical properties of composites; e.g., high aspect ratios contribute to greater reduction in thermal expansion.[1,60a] The high value of the thermal expansion coefficient of polymers is caused by the low energy barrier for the chain conformation to be changed. The thermal expansion coefficient always decreases with increasing aspect ratio and filler loading due to the mechanical constraint of the filler. Enhancement of dimensional stability is expected when a filler with high modulus and low thermal expansion coefficient is dispersed in a matrix of lower modulus and higher thermal expansion coefficient owing to simple mechanical restraints. Layered silicates seem attractive for this purpose owing to their high modulus, high aspect ratio, and low coefficient of thermal expansion; in addition, they are likely to be less detrimental to surface finish and ductility than conventional fillers. The larger constraining effect imposed by dispersed rigid platelets translates into lower thermal expansion coefficients.

The rate of CTE decreasing with increasing clay content is slightly higher for polymers with smaller chains. This observation can be rationalized by considering that, for a given MT loading, the corresponding low molecular weight PEO fractions, characterized by higher chain mobility, should suffer the larger constraining effects imposed by dispersed rigid platelets more than their longer counterparts, and this ultimately translates onto lower thermal expansion coefficients for lower DP PEO/MMT PCNs. Notably, above a certain filler content (between 6 and 8%), the CTE values for all PNCs seems to converge, suggesting that the effect of the polymer molecular mass levels off when a substantial amount of filler is present, and polymer chains undergo comparable constraining effects imposed by the mineral particles independently on their relative length.

Figure 6b shows the behavior of electrical conductivity σ for all PEO/MMT PCNs as a function of clay loading, as estimated with our multiscale simulation procedure. Although the effect of polymer molecular weight on σ is less pronounced than in the case of CTE, we can still observe that, in particular at lower clay contents, PNCs with shorter PEO chains features higher values of σ with respect to high molecular weight samples. Intuitively, this can be ascribed once more to the higher mobility of smaller PEO chains but, importantly, also to the lower affinity of these shorter macromolecules for the MMT surface (see Table 3, Figure 1, and discussion above). MMT samples in equilibrium with the atmospheric moisture have water molecules associated with the interlayer cations; accordingly, the enhanced ionic conductivity of these systems can be mainly ascribed to the interlayer cations associated with water molecules.[52] By interacting less tightly with the clay platelet, and being distributed mainly at the center of the interlayer galleries, the low DP PEO chains allows for a higher mobility of the interlayer cations and their hydration shell. In the presence of high molecular weight chains, on the contrary, the high affinity of these macromolecules for the clay surface, and the tendency to adopt chain conformations which maximize polymer segments/clay platelet interactions, ultimately produce a strong association of the interlayer cations and the clay surface oxygens. As a consequence, these metal ions remain entrapped into a highly constrained system where their mobility is prevented, and very high temperatures (e.g., up to 600 K) are required to observe ionic conductivity in the range 10^{-8}−10^{-9} S/cm.[7]

PEO intercalation into the MMT galleries, coupled with the presence of water molecules in the sheet spacing produce drastic cation environment modifications that allow appreciable electric conductivity even at ordinary temperature. Following Aranda,[7] and in harmony with the morphologies predicted at all scales in this work, in water-PEO intercalated PCNs the organic polymers with smaller mass chains, by maximizing their density in the interlayer spacing, act as a sort of pillar, causing a permanent separation between the silicate layers on one side and, on the other, reducing the cations mobility restrictions. In addition to this so-called "pillar-effect", other factors, mainly associated with the relaxation of the polymer chains, can also concur to the increase of the cation mobility,[61] although a detailed discussion on these effects is outside the scope of the present paper.

3. Conclusions

There are many levels at which computer-based molecular simulation techniques can be useful, ranging from highly detailed *ab initio* quantum mechanics, through classical, atomistic molecular dynamics, to process engineering modeling. These computations can significantly contribute to reduce wasted experiments, allow products and processes to be optimized, and permit large numbers of candidate materials to be screened *a priori*, even before their synthesis. These techniques are currently used to obtain thermodynamic information about pure or mixed systems. This information obtained by using microscopic properties assumes any system to be homogeneous in composition, structure and density, which is clearly a severe limitation. When a system is complex, comprising several components, eventually sparingly miscible, PCNs being prime examples, peculiar phases with remarkable properties can be observed. These so-called mesophases comprise far too many atoms for atomistic modeling description. Hence, coarse-grained methods are better suited to simulate such structures. One of the primary techniques for mesoscopic modeling is DPD, a particle-based method that uses soft-spheres to represent groups of atoms, and incorporates hydrodynamic behavior via a random noise, which is coupled to a pairwise dissipation. However, retrieving information on mesophase structures is not enough for predicting macroscopic features of such materials. This is possible if mesophase modeling is coupled with appropriate finite element tools like Palmyra that—provided properties of pure components are given or can be in turn obtained by simulation—allow obtaining a realistic estimation of many nanocomposites features, if integrated with experimental/simulated morphological data.

In this work we presented the derivation and application of a multiscale molecular modeling procedure to characterize polymer−clay nanocomposite materials obtained from water solution intercalation. This approach relies on a step-by step message-passing technique from atomistic to mesoscale to finite element level; thus, computer simulations at all scales are completely integrated, and virtually no experimental data are necessary to characterize the systems, at least at a preliminary stage of the analysis.

The entire computational procedure has been applied to four PCN systems based on montmorillonite and poly(ethylene oxide) with different molecular weights as test materials, and their thermal and electrical macroscopical properties were predicted in excellent agreement with the available experimental data.

The global perspective of our current research in this field is the complete integration of all available simulation scales, in a hierarchical procedure, to provide an efficient and robust simulation protocol for the successful design of PCNs of industrial interest, and the prediction of their final performance. Although the proposed computational recipe could still be refined by considering, for instance, a more precise analysis of different morphologies, matrix morphology next to the single exfoliated platelet surface, and exfoliation rate (issues that are currently being addressed by our group), to our knowledge this is the first, successful computational procedure applied to water-based PCNs able to predict, with a high degree of confidence, PCNs hierarchical structures and behavior, and to capture all the phenomena taking place on length scales that typically span 5−6 orders of magnitude and time scales encompassing a dozen of orders of magnitude.

References and Notes

(1) (a) Pinnavaia, T. J.; Beall, G. W. *Polymer-clay nanocomposites*: John Wiley & Sons Ltd.: Chichester, England, 2001. (b) Biswas, M.; Sinha Ray, S. *Adv. Polym. Sci.* **2001**, *155*, 167–221. (c) Sinha Ray, S.; Okamoto, M. *Prog. Polym. Sci.* **2003**, *28*, 1539–1641. (d) Utraki, L. A. *Clay-containing polymeric nanocomposites*: Rapra Technology: Shrewsbury, England, 2004. (e) Zeng, Q. H.; Yu, A. B.; Lu, G. Q.; Paul, D. R. *J. Nanosci. Nanotechnol.* **2005**, *5*, 1574–1592. (f) Balazs, A. C.; Emrick, T.; Russell, T. P. *Science* **2006**, *314*, 1107–1110. (g) Pavlidou, S.; Papaspyrides, C. D. *Prog. Polym. Sci.* **2008**, *33*, 1119–1198. (h) Paul, D. R.; Robeson, L. M. *Polymer* **2008**, *49*, 3187–3204.

(2) Zeng, Q. H.; Yu, A. B.; Lu, G. Q. *Prog. Polym. Sci.* **2008**, *33*, 191–269.

(3) Aranda, P.; Ruiz-Hitzky, E. *Chem. Mater.* **1992**, *4*, 1395–1403.

(4) Greenland, D. J. *J. Colloid Sci.* **1963**, *18*, 647–664.

(5) Kim, S.; Hwang, E.-J.; Jung, Y.; Han, M.; Park, S.-J. *Colloids Surf., A* **2008**, *313−314*, 216–219.

(6) Wu, J.; Lerner, M. M. *Chem. Mater.* **1993**, *5*, 835–838.

(7) Aranda, P.; Ruiz-Hitzky, E. *Chem. Mater.* **1992**, *4*, 1395–1403.

(8) Vaia, R. A.; Vasudevan, S.; Krawiec, W.; Scanlon, L. G.; Giannelis, E. P. *Adv. Mater.* **1995**, *7*, 154–156.

(9) Chaiko, D. J. *Chem. Mater.* **2003**, *15*, 1105–1110.

(10) Pozzo, D. C.; Walker, L. M. *Colloids Surf. A.* **2004**, *240*, 187–197.

(11) Armand, M. B.; Chabagno, J. M.; Duclot, M. J. In *Fast ionic transport in solids*; Vashishta, M., Ed.; Elsevier: Amsterdam, The Netherlands, 1979.

(12) (a) Aabloo, A.; Thomas, J. *Solid State Ionics* **2001**, *143*, 83–87. (b) Catlow, C. R. A.; Mills, G. E. *Electrochim. Acta* **1995**, *40*, 2057–2062. (c) Ferreira, B. A.; Müller-Plathe, F.; Bernardes, A. T.; De Almeida, W. B. *Solid State Ionics* **2002**, *147*, 361–366.

(13) de Leeuw, S. W.; van Zon, A.; Bel, G. J. *Electrochim. Acta* **2001**, *46*, 1419–1426.

(14) de Jonge, J. J.; van Zon, A.; de Leeuw, S. W. *Solid State Ionics* **2002**, *147*, 349–359.

(15) Kasemägi, H.; Klintenberg, M.; Aabloo, A.; Thomas, J. O. *Electrochim. Acta* **2003**, *48*, 2273–2278.

(16) Ferreira, B. A.; Dos Santos, H. F.; Bernardes, A. T.; Silva, G. G.; De Almeida, W. B. *Chem. Phys. Lett.* **1999**, *307*, 95–101.

(17) van Zon, A.; Mos, B.; Verkerk, P.; de Leeuw, S. W. *Electrochim. Acta* **2001**, *46*, 1717–1721.

(18) Karo, J.; Aabloo, A.; Thomas, J. O. *Solid State Ionics* **2005**, *176*, 3041–3044.

(19) Aabloo, A.; Klintenberg, M.; Thomas, J. O. *Electrochim. Acta* **2000**, *45*, 1425–1429.

(20) (a) Kasemägi, H.; Aabloo, A.; Klintenberg, M. K.; Thomas, J. O. *Solid State Ionics* **2004**, *168*, 249–254. (b) Kasemägi, H.; Klintenberg, M. K.; Aabloo, A.; Thomas, J. O. *Solid State Ionics* **2002**, *147*, 367–375.

(21) Scocchi, G.; Posocco, P.; Fermeglia, M.; Pricl, S. *J. Phys. Chem. B* **2007**, *111*, 2143–2151.

(22) (a) Hoogerbruge, P. J.; Koelman, J. M. V. A. *Europhys. Lett.* **1992**, *18*, 155–160. (b) Koelman, J. M. V.A.; Hoogerbruge, P. J. *Europhys. Lett.* **1993**, *21*, 363.

(23) (a) Fermeglia, M.; Ferrone, M.; Pricl, S. *Fluid Phase Equilbr.* **2003**, *212*, 315–329. (b) Toth, R.; Coslanich, A.; Ferrone, M.; Fermeglia, M.; Pricl, S.; Miertus, S.; Chiellini, E. *Polymer* **2004**, *45*, 8075–8083. (c) Scocchi, G.; Posocco, P.; Danani, A.; Pricl, S.; Fermeglia, M. *Fluid Phase Equilibr.* **2007**, *261*, 366–374. (d) Fermeglia, M.; Ferrone, M.; Pricl, S. *Mol. Simul.* **2004**, *30*, 289–300. (e) Scocchi, G.; Posocco, P.; Handgraaf, J.-W.; Fraaije, J. G. E. M.;Fermeglia, M.; Pricl, S. *Chem.—Eur. J.* **2009**, in press, DOI: 10.1002/chem.200900995).

(24) (a) Heinz, H.; Suter, U. W. *J. Phys. Chem. B* **2004**, *108*, 18341–18352. (b) Heinz, H.; Koerner, H.; Anderson, K. L.; Vaia, R. A.; Farmer, B. L. *Chem. Mater.* **2005**, *17*, 5658–5669.

(25) (a) Brown, G. *The X-ray Identification and Crystal Structures of Clay Minerals*: Mineralogical Society: London, 1961. (b) *Reviews in Mineralogy*; Bayley, S. W., Ed.; Mineralogical Society of America: Chelsea, MI, 1988; Vol. *19*. See also http://www.webmineral.com; (c) Tsipurski, S. I.; Drits, V. A. *Clay Miner.* **1984**, *19*, 177–193. (d) The exact crystal structure of MMT depends on the nature of the cations (e.g., Na^{+}, K^{+}, Ca^{+2}), charge density, and the presence of crystal water. However, mainly the parameters c (approximately 9.9−13 Å) and β (approximately 95−100°) are affected.

(26) Flory, P. J. *Principles of Polymer Chemistry*; Cornell University Press: Ithaca, NY, 1974.

(27) Theodorou, D. N.; Suter, U. W. *Macromolecules* **1986**, *19*, 139–154.

(28) (a) Fermeglia, M.; Pricl, S. *AIChE J.* **1999**, *45*, 2619–2627. (b) Fermeglia, M.; Ferrone, M.; Pricl, S. *Bioorg. Med. Chem.* **2002**, *10*, 2471–2478. (c) Felluga, F.; Pitacco, G.; Valentin, E.; Coslanich, A.; Fermeglia, M.; Ferrone, M.; Pricl, S. *Tetrahedron: Asym.* **2003**, *14*, 3385–3399. (d) Pricl, S.; Fermeglia, M.; Ferrone, M.; Asquini, A. *Carbon* **2003**, *41*, 2269–2283. (e) Metullio, L.; Ferrone, M.; Coslanich,

A.; Fuchs, S.; Fermeglia, M.; Paneni, M. S.; Pricl, S. *Biomacromolecules* **2004**, *5*, 1371–1378. (f) Toth, R.; Ferrone, M.; Miertus, S.; Chiellini, E.; Fermeglia, M.; Pricl, S. *Biomacromolecules* **2006**, *7*, 1714–1719. (g) Fermeglia, M.; Cosoli, M.; Ferrone, M.; Piccarolo, S.; Mensitieri, G.; Pricl, S. *Polymer* **2006**, *47*, 5979. (h) Posocco, P.; Ferrone, M.; Fermeglia, M.; Pricl, S. *Macromolecules* **2007**, *40*, 2257–2266. (i) Mensitieri, G.; Larobina, D.; Guerra, G.; Venditto, V.; Fermeglia, M.; Pricl, S. *J. Polym. Sci., B: Polym. Phys.* **2008**, *46*, 8. (j) Cosoli, P.; Scocchi, G.; Pricl, S.; Fermeglia, M. *Microporous Mesoporous Mater.* **2008**, *1*, 169.

(29) Tanaka, G.; Goettler, L. A. *Polymer* **2002**, *43*, 541–553.

(30) Gardebien, F.; Bredas, J.-L.; Lazzaroni, R. *J. Phys. Chem. B* **2005**, *109*, 12287–12296.

(31) Katti, K. S.; Sikdar, D.; Katti, D. R.; Ghosh, P.; Verma, D. *Polymer* **2006**, *47*, 403–414.

(32) Paul, D. R.; Zeng, Q. H.; Yu, A. B.; Lu, G. Q. *J. Colloid Interface Sci.* **2005**, *292*, 462–468.

(33) Berendsen, H. J. C.; Grigera, J. R.; Straatsma, T. P. *J. Phys. Chem.* **1987**, *91*, 6269–6271.

(34) Hackett, E.; Manias, E.; Giannelis, E. P. *Chem. Mater.* **2000**, *12*, 2161–2167.

(35) Bujdak, J.; Hackett, E.; Giannelis, E. P. *Chem. Mater.* **2000**, *12*, 2168–2174.

(36) Misra, S.; Fleming, P. D.III; Mattice, W. L. *J. Comp. Aided. Mater. Des.* **1995**, *2*, 101–112.

(37) Heinz, H.; Paul, W.; Suter, U. W.; Binder, K. *J. Chem. Phys.* **2004**, *120*, 3847–3854.

(38) Yang, D.-K.; Zax, D. B. *J. Chem. Phys.* **1999**, *110*, 5325–5336.

(39) Ewald, P. P. *Ann. Phys.* **1921**, *64*, 253–287.

(40) Nosé, S. *Prog. Theor. Phys., Suppl.* **1991**, *103*, 1–46.

(41) Groot, R. D.; Warren, P. B. *J. Chem. Phys.* **1997**, *107*, 4423–4435.

(42) Connolly, M. L. *J. Am. Chem. Soc.* **1985**, *107*, 1118–1124.

(43) Kawaguchi, S.; Imai, G.; Suzuki, J.; Miyahara, A.; Kitano, T.; Ito, K. *Polymer* **1997**, *38*, 2885–2891.

(44) Smith, G. D.; Yoon, D. Y.; Jaffe, R. L.; Colby, R. H.; Krishnamoorti, R.; Fetters, L. J. *Macromolecules* **1996**, *29*, 3462–3469.

(45) Blomqvist, J.; Mietila, L.-O.; Mannfors, B. *Polymer* **2001**, *42*, 109–116.

(46) Maly, M.; Posocco, P.; Pricl, S.; Fermeglia, M. *Ind. Eng. Chem. Res.* **2008**, *47*, 5023–5038.

(47) Annis, B. K.; Kim, M.-H.; Wignall, G. D.; Borodin, O.; Smith, G. D. *Macromolecules* **2000**, *33*, 7544–7548.

(48) Dong, H.; Hyun, J.-K.; Durham, C.; Wheeler, R. A. *Polymer* **2001**, *42*, 7809–7817.

(49) Lavallee, P.; Boon, J. P.; Noullez, A. *Physica D* **1991**, *47*, 233–240.

(50) Osman, M. A.; Mittal, V.; Lusti, H. R. *Macromol. Rapid Commun.* **2004**, *25*, 1145–1149.

(51) Heggli, M.; Etter, T.; Wyss, P.; Uggowitzer, P. J.; Gusev, A. A. *Adv. Eng. Mater.* **2005**, *7*, 225–229.

(52) (a) Fripiat, J. J.; Jelli, A.; Poncelet, G.; André, J. *J. Phys. Chem.* **1965**, *69*, 2185–2196. (b) McGowan, J. C. *Polymer* **1969**, *10*, 841–848. (c) Wu, J.; Lerner, M. M. *Chem. Mater.* **1993**, *5*, 835–838. (d) Shanmukaraj, D.; Murugan, R. *J. Polym. Sci.* **2005**, *149*, 90–95. (e) Wang, W.; Yang, X.; Fang, Y.; Ding, J.; yan, J. *Appl. Energy* **2009**, *86*, 1196–1200. (f) Sengwa, R. J.; Choudhary, S.; Sankhla, S. *Colloids Surf., A* **2009**, *336*, 79–87.

(53) Fornes, T. D.; Hunter, D. L.; Paul, D. R. *Macromolecules* **2004**, *37*, 1793–1798.

(54) (a) Krishnamoorti, R.; Vaia, R. A.; Giannelis, E. P. *Chem. Mater.* **1996**, *8*, 1728–1734. (b) Harris, D. J.; Bonagamba, T. J.; Schmidt-Rohr, K. *Macromolecules* **1999**, *32*, 6718–6724. (c) Shen, Z.; Simon, G. P.; Cheng, Y.-B. *Polymer* **2002**, *43*, 4251–4260. (d) Chaiko, F. J. *Chem. Mater.* **2003**, *15*, 1105–1110. (e) Reinholdt, M. X.; Kirkpatrick, R. J.; Pinnavaia, T. J. *J. Phys. Chem. B* **2005**, *109*, 16296–16303. (f) Chen, B.; Evans, J. R. G. *J. Phys. Chem. B* **2004**, *108*, 14986–14990. (g) Sun, L.; Ertel, E. A.; Zhu, L.; Hsiao, B. S.; Avila-Orta, C. A.; Sics, I. *Langmuir* **2005**, *21*, 5672–5676.

(55) Gusev, A. A. *Macromolecules* **2001**, *34*, 3081–3093.

(56) Burchill, S.; Hall, P. L.; Harrison, R.; Hayes, M. H. B.; Langford, J. I.; Livingston, W. R.; Smedley, R. J.; Ross, D. K.; Tuck, J. J. *Clay Miner.* **1983**, *18*, 373–397.

(57) Yan, L. B.; Roth, C. B.; Low, P. F. *J. Colloid Interface Sci.* **1996**, *184*, 663–670.

(58) Coppin, F.; Berger, G.; Bauer, A.; Castet, S.; Loubet, M. *Chem. Geol.* **2002**, *182*, 57–68.

(59) (a) Kuppa, V.; Menakanit, S.; Krishnamoorti, R.; Manias, E. *J. Polym. Sci., B: Polym. Phys.* **2003**, *41*, 3285–3298. (b) Strawhecker, K. E.; Manias, E. *Chem. Mater.* **2003**, *15*, 844–849. (c) Loyens, W.; Jannasch, P.; Maurer, F. H. J. *Polymer* **2005**, *46*, 903–914. (d) Elmahdy, M. M.; Chrissopoupou, K.; Afratis, A.; Floudas, G.; Anastasiadis, S. H. *Macromolecules* **2006**, *39*, 5170–5173. (e) Mazo, M. A.; Manevitch, L. I.; Gusarova, E. B.; Shamaev, M. Y.; Berlin, A. A.; Balabaev, N. K.; Rutledge, G. C. *J. Phys. Chem. B* **2008**, *112*, 3597–3604.

(60) (a) Yoon, P. J.; Fornes, T. D.; Paul, D. R. *Polymer* **2002**, *43*, 6727–6741. (b) Jan, I.-N.; Lee, T.-M.; Chiou, K.-C.; Lin, J.-J. *Ind. Eng. Chem. Res.* **2005**, *44*, 2086–2090. (c) Lee, K. Y.; Kim, K. H.; Jeoung, S. K.; Ju, S. I.; Shim, J. H.; Kim, N. H.; Lee, S. G.; Lee, S. M.; Lee, J. K.; Paul, D. R. *Polymer* **2007**, *48*, 4174–4183. (d) Lee, K. Y.; Hong, S. R.; Jeoung, S. K.; Kim, N. H.; Lee, S. G.; Paul, D. R. *Polymer* **2008**, *49*, 2146–2152. (e) Rao, Y. Q.; Blanton, T. N. *Macromolecules* **2008**, *41*, 935–941.

(61) (a) Papke, B. L.; Ratner, M. A.; Shriver, D. F. *J. Electrochem. Soc.* **1982**, *129*, 1694–1701. (b) Ratner, M. A.; Shriver, D. F. *Chem. Rev.* **1988**, *88*, 109–124. (c) Cowie, J. M. G.; Cree, S. H. *Annu. Rev. Phys. Chem.* **1989**, *40*, 85–113.